

Geophysical Research Letters*

RESEARCH LETTER

10.1029/2024GL109247

Key Points:

- Measurements of iodine monoxide radicals at Storm Peak Laboratory are up to three times higher than predicted by GEOS-Chem
- IO tropospheric column variability is significant and highlights a need to better understand sources and sinks of tropospheric iodine
- Iodine may rival bromine as a tropospheric mercury oxidant; iodinemercury chemistry is understudied and missing in atmospheric models

Supporting Information:

Supporting Information may be found in the online version of this article.

Correspondence to:

R. Volkamer, rainer.volkamer@colorado.edu

Citation:

Lee, C. F., Elgiar, T., David, L. M., Wilmot, T. Y., Reza, M., Hirshorn, N., et al. (2024). Elevated tropospheric iodine over the central continental United States: Is iodine a major oxidant of atmospheric mercury? *Geophysical Research Letters*, 51, e2024GL109247. https://doi.org/10.1029/2024GL109247

Received 14 MAR 2024 Accepted 22 JUL 2024

Author Contributions:

Conceptualization: S. N. Lyman,
A. G. Hallar, L. E. Gratz, R. Volkamer
Data curation: R. Volkamer
Formal analysis: C. F. Lee, R. Volkamer
Funding acquisition: R. Volkamer
Investigation: C. F. Lee, T. Elgiar,
L. M. David, T. Y. Wilmot, M. Reza,
N. Hirshorn, S. N. Lyman, A. G. Hallar,
L. E. Gratz, R. Volkamer
Methodology: C. F. Lee, R. Volkamer

Resources: I. B. McCubbin, J. C. Lin Software: J. C. Lin Supervision: R. Volkamer Visualization: C. F. Lee

© 2024. The Author(s).

This is an open access article under the terms of the Creative Commons
Attribution-NonCommercial-NoDerivs
License, which permits use and
distribution in any medium, provided the original work is properly cited, the use is non-commercial and no modifications or adaptations are made.

Elevated Tropospheric Iodine Over the Central Continental United States: Is Iodine a Major Oxidant of Atmospheric Mercury?

C. F. Lee^{1,2} , T. Elgiar³, L. M. David^{3,4} , T. Y. Wilmot⁵ , M. Reza^{1,2}, N. Hirshorn^{5,6}, I. B. McCubbin⁵, V. Shah⁷ , J. C. Lin⁵ , S. N. Lyman^{3,8}, A. G. Hallar⁵ , L. E. Gratz^{9,10} , and R. Volkamer^{1,2}

¹Department of Chemistry, University of Colorado Boulder, Boulder, CO, USA, ²Cooperative Institute for Research in Environmental Sciences, Boulder, CO, USA, ³Bingham Research Center, Utah State University, Vernal, UT, USA, ⁴Now at Ramboll, Fort Collins, CO, USA, ⁵Department of Atmospheric Sciences, University of Utah, Salt Lake City, UT, USA, ⁶Now at Ramboll, New York, NY, USA, ⁷NASA Global Modeling and Assimilation Office and Science Systems and Applications, Inc, Greenbelt, MD, USA, ⁸Department of Chemistry & Biochemistry, Utah State University, Logan, UT, USA, ⁹Environmental Studies Program, Colorado College, Colorado Springs, CO, USA, ¹⁰Now at Department of Chemistry and Environmental Studies Program, Reed College, Portland, OR, USA

Abstract Previous efforts to measure atmospheric iodine have focused on marine and coastal regions. We report the first ground-based tropospheric iodine monoxide (IO) radical observations over the central continental United States. Throughout April 2022, IO columns above Storm Peak Laboratory, Colorado (3,220 m.a.s.l.) ranged from 0.7 ± 0.5 to $3.6 \pm 0.5 \times 10^{12}$ (average: 1.9×10^{12} molec cm⁻²). IO was consistently elevated in air masses transported from over the Pacific Ocean. The observed IO columns were up to three times higher and the range was larger than predicted by a global model, which warrants further investigation into iodine sources, sinks, ozone loss, and particle formation. IO mixing ratios increased with altitude. At the observed levels, iodine may be competitive with bromine as an oxidant of elemental mercury at cold temperatures typical of the free troposphere. Iodine-induced mercury oxidation is missing in atmospheric models, understudied, and helps explain model underestimation of oxidized mercury measurements.

Plain Language Summary Halogens such as chlorine, bromine, and iodine are highly reactive gases that participate in atmospheric chemistry, including ozone destruction, particle formation, modification of greenhouse gas lifetime (i.e., methane, dimethylsulfide), and the oxidation of elemental mercury. Iodine mainly enters the atmosphere from oceans; therefore, past measurements of atmospheric iodine have focused on marine and polar regions. This study describes the first lower atmospheric measurements of iodine monoxide (IO) radicals at a remote mountaintop site in the central continental United States. These measurements indicate that the concentration of IO radicals showed a large range over the course of 1 month and reached levels up to three times higher than predicted by a global atmospheric chemistry model. These observations suggest that our understanding of the iodine sources and sinks to the free troposphere may be incomplete. Moreover, we suggest that iodine's contribution to ozone destruction and mercury chemistry may be underestimated; in particular, iodine may be competitive with bromine in the oxidation of elemental mercury in the free troposphere.

1. Introduction

Atmospheric iodine destroys ozone (Koenig et al., 2020, 2021; Read et al., 2008; Saiz-Lopez et al., 2012, 2014; Sherwen et al., 2017), forms new particles (Baccarini et al., 2020; Finkenzeller et al., 2023; Gómez Martín et al., 2022; He et al., 2021; O'Dowd et al., 2002; Sipilä et al., 2016), and modifies atmospheric oxidative capacity (Sherwen, Evans, et al., 2016; Sherwen, Schmidt, et al., 2016). Iodine mainly enters the atmosphere in inorganic gaseous form (HOI, I₂) through reaction with ozone at the ocean surface (Carpenter et al., 2013; MacDonald et al., 2014; Wang et al., 2021), with smaller sources from organic iodine species (Bell et al., 2002; Jones et al., 2010; Ordóñez et al., 2012; Sive et al., 2007; Wang et al., 2021), windblown dust (Koenig et al., 2021; Williams et al., 2007), and volcanic eruptions (Schönhardt et al., 2017). Tree ring and ice core records indicate that atmospheric iodine has increased threefold since 1950, which is attributed to increased anthropogenic surface ozone pollution resulting in increased marine iodine emissions (Cuevas et al., 2018; Legrand et al., 2018; Zhao et al., 2019).

LEE ET AL. 1 of 13

Writing – original draft: C. F. Lee, R. Volkamer Writing – review & editing: T. Elgiar, L. M. David, T. Y. Wilmot, M. Reza, N. Hirshorn, V. Shah, J. C. Lin, S. N. Lyman, A. G. Hallar, L. E. Gratz Most of our knowledge about the global distribution of atmospheric iodine is from measurements of iodine monoxide (IO) radicals in the marine boundary layer (Alicke et al., 1999; Allan et al., 2000; Coburn et al., 2011; Furneaux et al., 2010; Gómez Martín et al., 2013; Großmann et al., 2013; Inamdar et al., 2020; Mahajan et al., 2012; Prados-Roman et al., 2015; Takashima et al., 2022; Wang et al., 2014; Whalley et al., 2007) and at high latitudes (Frieß et al., 2010; Mahajan et al., 2010; Schönhardt et al., 2012, 2017; Wittrock et al., 2000). Recent evidence of IO in the free troposphere is limited to measurements over oceans (Dix et al., 2013; Koenig et al., 2021; Puentedura et al., 2012; Volkamer et al., 2015; Wang et al., 2015). IO in the tropical transition layer (Volkamer et al., 2015) and lower stratosphere (Koenig et al., 2020) suggests that iodine is globally distributed. Despite the limited spatiotemporal coverage of existing IO measurements, the ability of the GEOS-Chem model to accurately reproduce IO vertical profile measurements over the Pacific Ocean (Volkamer et al., 2015; Wang et al., 2021) suggests that our understanding of atmospheric iodine chemistry is well-constrained near marine sources. However, there is a distinct lack of IO measurements over the center of continents, far from marine sources, where IO sinks become more important.

To our knowledge, there is no previous ground-based measurement of tropospheric IO over the continental United States. The only previous attempt to measure IO from the continental U.S. was by Wennberg et al. (1997), who measured IO slant column densities (SCDs) during three sunrises at Kitt Peak, Arizona, with a solar geometry that maximized sensitivity to stratospheric IO but minimized sensitivity to tropospheric IO; they did not attempt to quantify tropospheric IO. Therefore, tropospheric IO over the center of the continental U.S. is unconstrained by ground-based measurements.

Mountaintop Multi-AXis Differential Optical Absorption Spectroscopy (MAX-DOAS) is well-suited for tropospheric IO measurements because it maximizes measurement sensitivity by minimizing aerosol scattering effects, provides access to the free troposphere due to the extended spatial scale (tens of kilometers) of the measurement light path, and enables cost-effective long-term measurements compared to airborne campaigns. Mountaintop MAX-DOAS has been successfully employed for IO measurements in the marine free troposphere (Puentedura et al., 2012).

The role of iodine radicals as oxidants of atmospheric mercury is understudied. Mercury enters the atmosphere mainly in gaseous elemental form, $\operatorname{Hg^0}_{(g)}$, where it is oxidized into short-lived $\operatorname{Hg^I}(X)_{(g)}$ species ($X = \operatorname{Br}$, OH , CI) and then stabilized through secondary oxidation reactions to form $\operatorname{Hg^I}_{(g)}$ species, including $\operatorname{Hg^I}(\operatorname{Br})(\operatorname{OH})$ and $\operatorname{Hg^I}(\operatorname{OH})_2$ (Castro et al., 2022; Dibble et al., 2020; Shah et al., 2021). The oxidation of $\operatorname{Hg^0}_{(g)}$ by atmospheric iodine radicals has been deemed unimportant due to the low amounts of tropospheric iodine and the much faster thermal decomposition of $\operatorname{Hg^I}(I)_{(g)}$ compared to $\operatorname{Hg^I}(\operatorname{Br})_{(g)}$ (Cremer et al., 2008; Goodsite et al., 2004, 2012; Shepler et al., 2005). Accordingly, the latest implementation of atmospheric mercury chemistry in the GEOS-Chem model does not include reactions involving iodine (Shah et al., 2021). However, mercury measurements in aerosols are empirically correlated with iodine (Murphy et al., 2006). Additionally, the fast, barrierless reaction of $\operatorname{Hg^I}$ species with ozone (Saiz-Lopez et al., 2020) can compete with the thermal decomposition of $\operatorname{Hg^I}(I)_{(g)}$, prompting us to re-evaluate the importance of iodine as an $\operatorname{Hg^0}_{(g)}$ oxidant.

Here we present one month (April 1–30, 2022) of MAX-DOAS measurements of IO, H_2O , NO_2 , and HCHO tropospheric vertical column densities (VCD_{trop}) and volume mixing ratios at instrument altitude (VMR_{instr}) alongside co-located in-situ measurements of $Hg^0_{(g)}$ and $Hg^{II}_{(g+p)}$ at a remote mountaintop observatory in the central continental U.S. Section 2 describes the measurement site and methods. Section 3 presents the first ground-based observational constraint on tropospheric IO over the central continental U.S., explores correlations, and compares observations with a global model. Section 4 uses the observations to constrain a box model of gasphase mercury chemistry to investigate the relevance of iodine radicals for $Hg^0_{(g)}$ oxidation and discusses atmospheric implications.

2. Methods

2.1. Storm Peak Laboratory

Storm Peak Laboratory (SPL) is a mountaintop observatory on top of the continental divide in the Rocky Mountains in northwestern Colorado (3,220 m.a.s.l, 40.455°N, 106.745°W). SPL has been an atmospheric research station since the 1980s (Borys & Wetzel, 1997; Hallar et al., 2016) and has been previously used for

LEE ET AL. 2 of 13

atmospheric mercury measurements (Fain et al., 2009; Obrist et al., 2008). All measurements presented here were conducted at SPL from April 1–30, 2022.

2.1.1. CU MAX-DOAS

The University of Colorado MAX-DOAS (CU MAX-DOAS) instrument (Coburn et al., 2011, 2016) measured ultraviolet-visible scattered-light solar spectra at different elevation angles in a single azimuthal viewing direction. Trace gas differential slant column densities (dSCDs) were retrieved from solar spectra using the DOAS method (Platt & Stutz, 2008). A cloud-free zenith reference spectrum (Gielen et al., 2014; Wagner et al., 2014) on 6 April 2022 at 18:00 UTC was used for all DOAS retrievals; fit settings are in Tables S1 & S2 in Supporting Information S1. IO, $\rm H_2O$, HCHO, and $\rm O_2\text{-}O_2$ dSCDs were converted into SCDs by adding the trace gas SCD in the reference spectrum (SCD_{ref}); past studies have shown that accounting for SCD_{ref} maximizes sensitivity in the free troposphere (Coburn et al., 2016; Hendrick et al., 2007) and avoids bias in the retrieval of columns and profiles (Volkamer et al., 2015). For NO₂, the stratospheric signal was removed by subtracting the zenith dSCDs from the off-axis dSCDs. A linear optimal estimation algorithm (Rodgers, 2000) was used to retrieve IO, NO₂, $\rm H_2O$, and HCHO VCD_{trop} and VMR_{instr} from the measured SCDs (zenith-subtracted dSCDs for NO₂). Instrument and retrieval details are in Text S1 in Supporting Information S1.

2.1.2. Dual-Channel Mercury System

A cation-exchange membrane-based dual-channel system to measure total gaseous elemental mercury, $\operatorname{Hg^0}_{(g)}$, and total gas- and particle-phase oxidized mercury, $\operatorname{Hg^I}_{(g+p)}$ (Derry et al., 2024; Elgiar et al., 2024; Lyman et al., 2020), pulled sample air through a heated PTFE Teflon-coated inlet with an elutriator and particle impactor (2.5 µm cut point), 50 cm of heated PFA Teflon line, to two separate measurement channels. A Tekran 2537X Hg vapor analyzer sampled from each channel sequentially. One channel included a series of two in-series cation exchange-membranes that have been shown to pass $\operatorname{Hg^0}_{(g)}$ and retain $\operatorname{Hg^II}_{(g+p)}$ (Miller et al., 2019); the other channel included a thermal converter that converted total atmospheric Hg to $\operatorname{Hg^0}_{(g)}$. $\operatorname{Hg^II}_{(g+p)}$ was calculated as the difference between the two channels every 10 minutes. The dual-channel system had a 1-hr $\operatorname{Hg^{II}}_{(g+p)}$ detection limit less than 15 pg m⁻³; total Hg and $\operatorname{Hg^0}_{(g)}$ are assumed to be similar. A NIST-traceable permeation tube-based calibrator was used to add $\operatorname{Hg^0}_{(g)}$ and $\operatorname{HgBr_2}_2$ to the inlet of the dual-channel system while it sampled ambient air, and the system recovered 97 \pm 4% and 100 \pm 9%, respectively (mean \pm standard deviation). The dual-channel system is described in detail in Elgiar et al. (2024).

2.2. Model Tools

2.2.1. GEOS-Chem

The GEOS-Chem 3-D atmospheric chemistry model was used to simulate (a) oxidant fields at $0.5^{\circ} \times 0.625^{\circ}$ and (b) mercury chemistry as described in Shah et al. (2021) at $2.0^{\circ} \times 2.5^{\circ}$. The GEOS-Chem halogen chemistry, including iodine, is implemented according to Wang et al. (2021), which represents emissions of HOI and I₂ from the ocean surface, as well as emissions of organic iodine. The chemistry of fourteen gas-phase inorganic and three organic iodine species are explicitly represented. The main sinks of iodine in the model are dry deposition, wet deposition, and uptake onto particles. Details are in Text S2 in Supporting Information S1. April 2022 daytime averages of GEOS-Chem oxidant fields and Hg^0 were used to constrain the gas-phase mercury box model described in Section 2.2.3.

2.2.2. HYSPLIT-STILT

The Hybrid Single-Particle Lagrangian Integrated Trajectory model coupled to the Stochastic Time-Inverted Lagrangian Transport Model (STILT; Lin et al., 2003; Loughner et al., 2021) was used to simulate air mass origin at SPL. One thousand 24-hr back trajectories were initiated at each of multiple altitudes (5 m, 2 km, 4 km, 6 km, 10 km above ground level) at SPL every 3 hr from April 1–30, 2022. At each initial altitude, the one thousand back-trajectories were averaged in three dimensions (latitude, longitude, altitude) to calculate a single back trajectory every three hours (Figure 1). Details are in Text S5 in Supporting Information S1.

LEE ET AL. 3 of 13

Residual

Measured IO

19448007, 2024, 17, Downloaded from https://agupubs.onlinelibrary.wiley.com/doi/10.1029/2024GL109247, Wiley Online Library on [06/09/2024]. See the Terms and Conditions (https://online

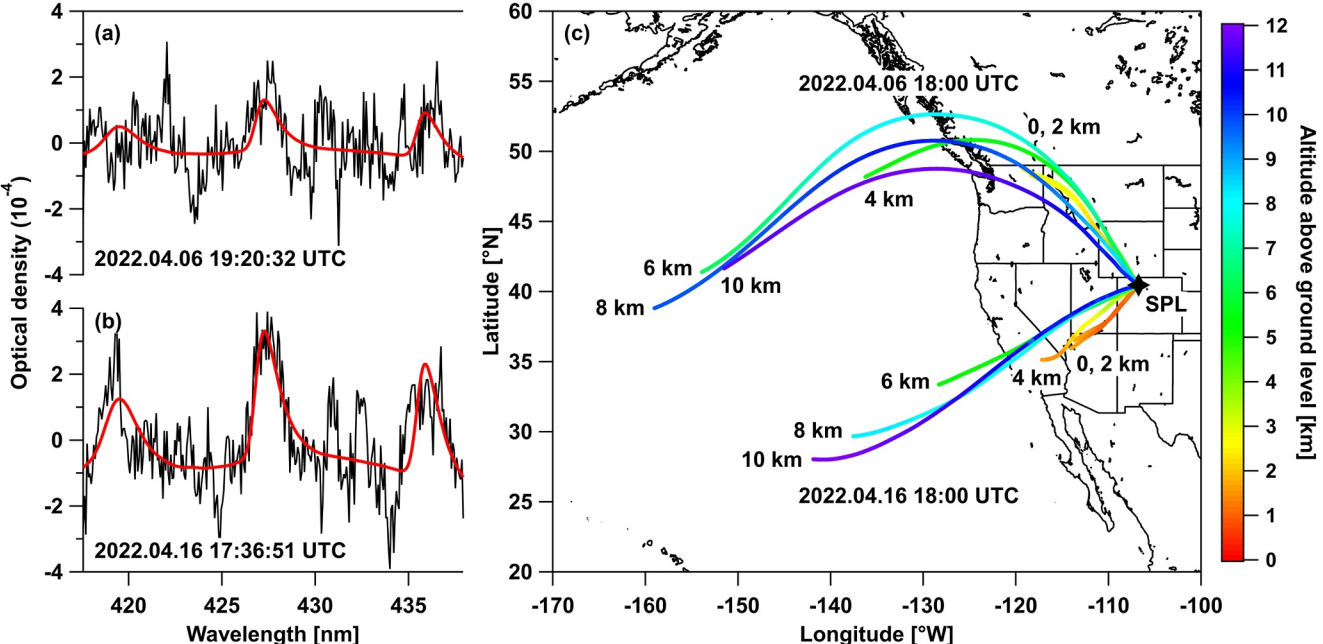


Figure 1. Detection of iodine monoxide (IO) radicals above Storm Peak Laboratory during April 2022. (a) IO spectral proof for a "low IO" case on April 6 at 19:20:32 UTC corresponding to $(0.6 \pm 0.1) \times 10^{13}$ molec cm⁻² IO differential slant column densitie (dSCD). (b) IO spectral proof for a "high IO" case on April 16 at 17:36:51 UTC corresponding to $(1.6 \pm 0.1) \times 10^{13}$ molec cm⁻² IO dSCD. (c) Average STILT 24-hr back trajectories for April 6 at 18:00 UTC and April 16 at 18:00 UTC.

2.2.3. Mercury Box Model

The Framework for 0-D Atmospheric Modeling (F0AM; Wolfe et al., 2016) version 4.2.2 was used to simulate gas-phase mercury chemistry in 1 km layers from the surface at 2-12 km. GEOS-Chem April 2022 daytime averages were used to constrain oxidant fields and Hg0; iodine radicals were scaled to the average observed IO column (I atom $VCD_{trop} = 9.9 \times 10^7$ molec cm⁻²; Text S4 in Supporting Information S1). The reaction mechanism used is based on Shah et al. (2021) with three significant differences; first, reactions involving I & IO were added analogously to reactions involving Br & BrO (Saiz-Lopez et al., 2018); second, the reaction coefficient used for $Hg^{IX} + O_3 \rightarrow Hg^{II}(X)(O) + O_2$ was the value for a barrierless reaction reported in Saiz-Lopez et al. (2020); third, only gas-phase reactions are treated here, as the goal is to examine the relative contributions of Br, OH, and I to $\mathrm{Hg}^0_{(g)}$ oxidation rates. $\mathrm{Hg}^{\mathrm{II}}_{(g)}$ deposition and particle-phase partitioning is not the focus of this study and deemed independent of $Hg^{II}_{(g)}$ chemical identity (Shah et al., 2021). Sensitivity studies were performed varying the rate for $Hg^0 + I + M \rightarrow Hg^I(I) + M$, where (a) $Hg^I(I)$ forms at half the rate as $Hg^I(Br)$; (b) Hg^I(I) forms at the same rate as Hg^I(Br); and (c) Hg^I(I) forms at twice the rate as Hg^I(Br). The bond strength of Hg^I(I) is uncertain (Cremer et al., 2008; Goodsite et al., 2004; Shepler et al., 2005); sensitivity studies were performed varying the Hg-I bond energy (8, 9.5, 11 kcal mol⁻¹) using Hg-Br and Hg-OH as references. Box model output was extracted at 15 minutes, after gas-phase equilibrium was reached (Figure S5 in Supporting Information S1). Results from a subset of sensitivity studies are presented in Figure 3; results from all sensitivity studies are in Figure S6 in Supporting Information S1. The complete reaction mechanism is in Tables S5 and S6 in Supporting Information S1.

2.2.4. Radiative Transfer Model

The 3D Monte Carlo Atmospheric Radiative Transfer Inversion Model (McArtim3; Deutschmann et al., 2011) was used to calculate weighting functions for trace gas profile inversions. Model settings are in Table S2 in Supporting Information S1. Weighting functions were calculated in a Rayleigh atmosphere using April 2022 average daytime temperature and pressure profiles from ECMWF CAMS reanalysis (Inness et al., 2019) and empirically scaled to match the measured O₂-O₂ SCD for each spectrum. This approach uses the known O₂-O₂ vertical profile to account for the effects of terrain and temporal atmospheric state variability (temperature,

LEE ET AL. 4 of 13

pressure, weak aerosols) on the measured photon path distribution (Ortega et al., 2016; Spinei et al., 2015; Tirpitz et al., 2021; Wagner et al., 2019; see Text S1 in Supporting Information S1).

3. Results

Here, observations of IO, $Hg^0_{(g)}$, and $Hg^{II}_{(g+p)}$ are described and compared with GEOS-Chem simulations. Pearson correlation coefficients (R) of less than 0.20 are referred to as having no correlation; R is reported alongside its standard error. Averages are reported alongside standard deviations.

3.1. Detection of IO in the Continental Free Troposphere

IO concentrations above the detection limit were consistently observed throughout the month; spectral proofs are shown in Figure 1. On April 16, the day with the highest IO signal, IO dSCDs of up to $(2.2 \pm 0.4) \times 10^{13}$ and $(1.6 \pm 0.1) \times 10^{13}$ molec cm⁻² were observed in the limb (EA = 0°) and zenith (EA = 90°) geometries, respectively. On April 6, the day with the lowest IO signal, IO dSCDs of up to $(1.4 \pm 0.4) \times 10^{13}$ and $(0.6 \pm 0.1) \times 10^{13}$ molec cm⁻² were observed in the limb and zenith geometries, respectively.

Sensitivity studies varying the a priori profile used for the IO column retrieval indicate that IO VMR increased with altitude. Two a priori profiles were tested: a "flat" profile with a constant 0.10 pptv IO throughout the atmosphere, and the GEOS-Chem April 2022 daytime average IO profile. The GEOS-Chem profile, in which IO VMR increases with altitude, consistently resulted in better agreement between measured and a posteriori simulated IO SCDs than the "flat" profile (Figure S2 in Supporting Information S1). Therefore, the GEOS-Chem profile was used in the IO retrieval as it is more physically representative of the measurements.

IO VCD_{trop} was $0.7-3.6 \times 10^{12}$ molec cm⁻², averaging $(1.9 \pm 0.6) \times 10^{12}$ molec cm⁻². IO VCD_{trop} error is 0.5×10^{12} molec cm⁻², with contributions from choice of a priori settings $(0.3 \times 10^{12} \, \mathrm{molec \, cm^{-2}})$, uncertainty in SCD_{ref} $(0.1 \times 10^{12} \, \mathrm{molec \, cm^{-2}})$, and method error (spectral fitting, radiative transfer modeling, optimal estimation; $0.1 \times 10^{12} \, \mathrm{molec \, cm^{-2}})$. IO VMR_{instr} was $0.00-0.16 \, \mathrm{pptv}$, averaging $0.08 \pm 0.03 \, \mathrm{pptv}$. IO VMR_{instr} error is $0.03 \, \mathrm{pptv}$, with contributions from choice of a priori settings $(0.01 \, \mathrm{pptv})$, uncertainty in SCD_{ref} (<0.01 pptv), and method error (spectral fitting, radiative transfer modeling, optimal estimation; $0.02 \, \mathrm{pptv}$). Uncertainty in the IO absorption cross section is 2%, and negligible (Spietz et al., 2005).

Twenty four-hour STILT back trajectories indicated that the observed air masses consistently originated from over the Pacific Ocean. The air mass observed during the day with the highest IO signal (April 16) originated from the southwest, toward the tropics (Figure 1c). The air mass observed during the day with the lowest IO signal (April 6) originated from the northwest, toward mid-latitudes. However, not all tropical air masses contained higher IO; on April 28, for example, the back-trajectories indicated an air mass originating even further south than on April 16, yet the IO VCD was significantly larger on April 16 than on April 28. While air mass origin alone cannot account for the observed IO variability, we consistently found higher IO in air masses with less than 24-hr transport time from the Pacific Ocean. This indicated that IO variability also depended on the strength of IO sinks along the transport path, which are not constrained in our analysis.

IO VCD $_{trop}$ and VMR $_{instr}$ were up to three times larger, and the range of IO VCD $_{trop}$ and VMR $_{instr}$ was larger than predicted by GEOS-Chem (Figure 2). GEOS-Chem daytime IO VCD $_{trop}$ was 0.3–1.5 × 10¹² molec cm $^{-2}$, averaging 0.8 ± 0.2 × 10¹² molec cm $^{-2}$, two times smaller than observed. GEOS-Chem daytime IO VMR $_{instr}$ was 0.0007–0.10 pptv, averaging 0.04 ± 0.02 pptv, also two times smaller than observed. There was no correlation between measured and modeled IO VCD $_{trop}$. There was a very weak but statistically significant anti-correlation between measured and modeled IO VMR $_{instr}$ (R: -0.20 ± 0.05 ; $p<1\times10^{-4}$). The two days with the lowest IO VCD $_{trop}$, April 6 and 26, showed reasonable agreement with GEOS-Chem. However, on all other days, IO VCD $_{trop}$ was significantly larger than predicted. The GEOS-Chem horizontal grid cell size (0.5° × 0.625°) is comparable to the tens of kilometers sampled by the MAX-DOAS light path. The similar magnitude of underestimation of IO VCD $_{trop}$ and VMR $_{instr}$ by GEOS-Chem provides evidence that IO VMR increased with altitude, since GEOS-Chem consistently simulated increasing IO VMR with altitude. One would expect the GEOS-Chem underestimation to be different between IO VCD $_{trop}$ and VMR $_{instr}$ if the measured profile shape was very different than modeled.

LEE ET AL. 5 of 13

19448007, 2024, 17, Downloaded from https://agupubs.onlinelibrary.wiley.com/doi/10.1039/2024GL109247, Wiley Online Library on [06/09/2024]. See the Terms and Conditions (https://onlinelibrary.wiley.com/terms-and-conditions) on Wiley Online Library for rules

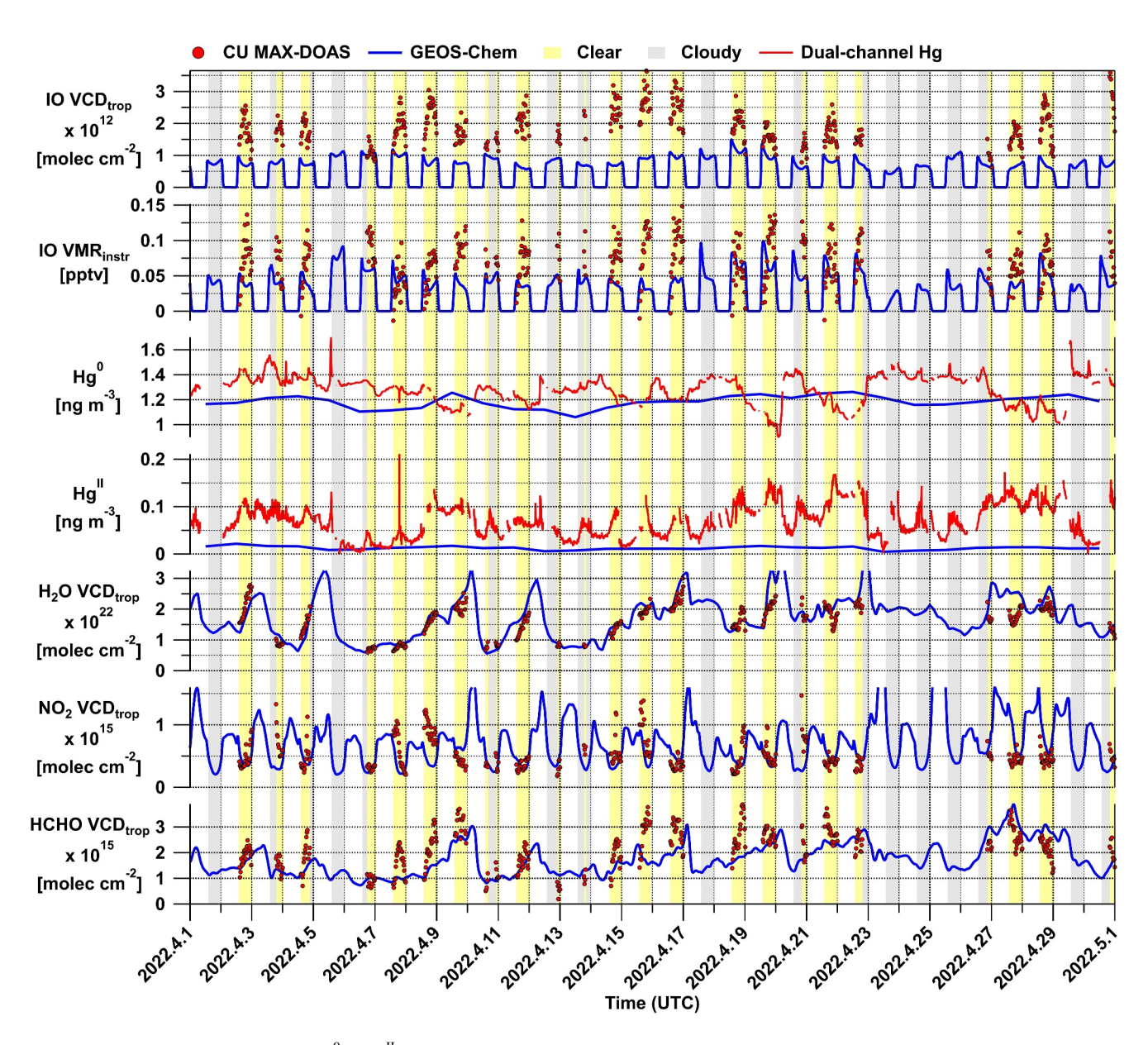


Figure 2. Measurements of iodine monoxide, $Hg^0_{(g)}$, $Hg^{II}_{(g+p)}$, H_2O , NO_2 , and HCHO at Storm Peak Laboratory are compared with GEOS-Chem during April 2022. VCD_{trop} was calculated from the surface to 12 km.

3.2. BrO

A measurement constraint on bromine was not possible during the study period. The amount of tropospheric BrO observed at SPL was consistently below the detection limit of \sim 0.5 pptv VMR $_{instr}$. The GEOS-Chem April 2022 daytime average BrO VMR $_{instr}$ at SPL was 0.15 pptv, consistent with the observations and too low to be observable even with the state-of-the-art MAX-DOAS instrument used here. We therefore used the GEOS-Chem BrO profile without modifications to constrain the mercury box model.

3.3. Mercury

 ${\rm Hg^0}_{(g)}$ was 0.90–1.70 ng m⁻³, averaging 1.28 \pm 0.11 ng m⁻³. ${\rm Hg^I}_{(g+p)}$ was 0–211 pg m⁻³, averaging 68 \pm 34 pg m⁻³. Interestingly, there was a weak anti-correlation between ${\rm Hg^0}_{(g)}$ and HCHO VMR $_{\rm instr}$ (R: -0.35 ± 0.05 ; $p < 1 \times 10^{-5}$), and a moderately strong correlation between ${\rm Hg^I}_{(g+p)}$ and HCHO VMR $_{\rm instr}$ (R:

LEE ET AL. 6 of 13

9448007, 2024, 17, Downloaded from https://agupubs.onlinelibrary.wiley.com/doi/10.1029/2024GL109247, Wiley Online Library on [0/6/99/2024]. See the Terms and Conditions (https://onlinelibrary.wiley.com/terms-and-conditions) on Wiley Online Library for rules of use; OA articles are governed by the applicable Creative

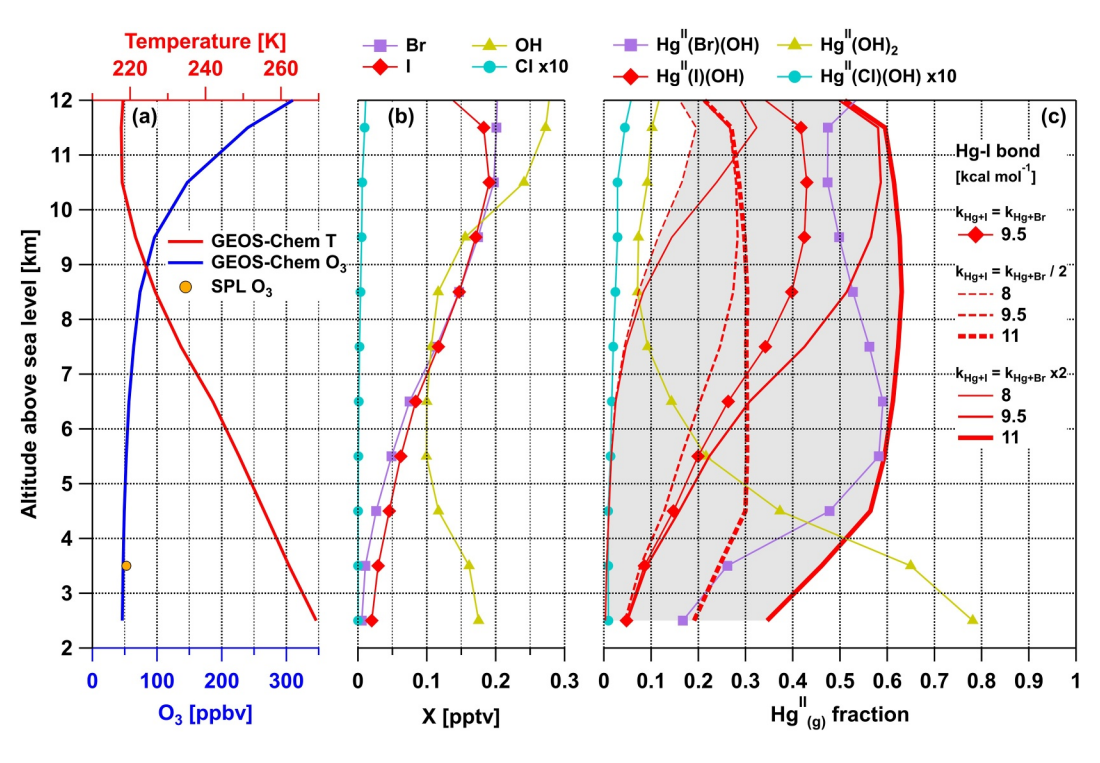


Figure 3. Iodine-initiated Hg^0 oxidation compared with other oxidation pathways above Storm Peak Laboratory (SPL). (a) GEOS-Chem temperature and ozone profiles used in the box model, alongside SPL ozone measurements. (b) Mercury oxidant profiles used in the box model. Br, OH, and Cl are from GEOS-Chem. The I atom profile (I $VCD_{trop} = 9.9 \times 10^7$ molec cm⁻²) is calculated from the measured monthly average iodine monoxide (IO) $VCD_{trop} = 10^{12}$ molec cm⁻²) using the GEOS-Chem I/IO ratio profile. (c) Box model results showing the fraction of $Hg^{II}_{(g)}$ produced via each oxidation pathway, varying the $Hg+I\leftrightarrow Hg^{I}(I)$ kinetics. $Hg^{II}(Br)(OH)$, $Hg^{II}(OH)_2$, and $Hg^{II}(Cl)(OH)$ are shown for the case assuming that $k_{Hg+I} = k_{Hg+Br}$ and that the Hg-I bond energy is 9.5 kcal mol^{-1} .

 0.64 ± 0.04 ; $p < 1 \times 10^{-5}$; Figure S4 in Supporting Information S1), indicating a possible connection between mercury oxidation and total atmospheric oxidative capacity.

Oxidized mercury at SPL coincided with warm air masses at low relative humidity, consistent with past work (Derry et al., 2024; Fain et al., 2009), but also at high absolute humidity. There was a weak anti-correlation between $\mathrm{Hg}^0_{(\mathrm{g})}$ and measured temperature (R: -0.37 ± 0.02 ; $p<1\times10^{-5}$), a strong correlation between $\mathrm{Hg}^{\mathrm{II}}_{(\mathrm{g+p})}$ and measured temperature (R: 0.70 ± 0.01 ; $p<1\times10^{-5}$; Figure S4 in Supporting Information S1), a weak correlation between $\mathrm{Hg}^0_{(\mathrm{g})}$ and measured relative humidity (R: 0.39 ± 0.02 ; $p<1\times10^{-5}$), a moderate anti-correlation between $\mathrm{Hg}^{\mathrm{II}}_{(\mathrm{g+p})}$ and measured relative humidity (R: -0.43 ± 0.01 ; $p<1\times10^{-5}$; Figure S4 in Supporting Information S1), and a weak correlation between $\mathrm{Hg}^{\mathrm{II}}_{(\mathrm{g+p})}$ and $\mathrm{H_2O}$ VMR_{instr} (R: 0.37 ± 0.04 ; $p<1\times10^{-5}$). This is consistent with the idea that mercury survives longer in air masses with less wet deposition, providing more time for oxidation to occur.

GEOS-Chem $\mathrm{Hg^0}_{(\mathrm{g})}$ was 1.06–1.26 ng m⁻³, averaging 1.18 \pm 0.05 ng m⁻³. GEOS-Chem $\mathrm{Hg^I}_{(\mathrm{g+p})}$ was 4–22 pg m⁻³, averaging 12 \pm 4 pg m⁻³. While measured and modeled $\mathrm{Hg^0}_{(\mathrm{g})}$ concentrations agreed reasonably well, there was no correlation in $\mathrm{Hg^0}_{(\mathrm{g})}$ temporal variability. Moreover, the measured $\mathrm{Hg^II}_{(\mathrm{g+p})}$ concentration was up to 10 times larger and more variable (i.e., a six times larger standard deviation) than modeled (Figure 2). Despite these differences, measured and modeled $\mathrm{Hg^{II}}_{(\mathrm{g+p})}$ were moderately correlated (R: 0.47 \pm 0.01; $p < 1 \times 10^{-5}$; Figure S4 in Supporting Information S1), indicating that GEOS-Chem had some skill in predicting $\mathrm{Hg^{II}}_{(\mathrm{g+p})}$ variability at SPL but not the magnitude. Increased $\mathrm{Hg^{II}}_{(\mathrm{g+p})}$ sources (i.e., iodine-induced oxidation) and/or decreased $\mathrm{Hg^{II}}_{(\mathrm{g+p})}$ sinks in the model are needed to explain this model-measurement disagreement.

LEE ET AL. 7 of 13

4.1. Literature Comparison

The observed IO VCD_{trop} monthly average of $1.9 \pm 0.6 \times 10^{12}$ molec cm⁻² over the central continental U.S. is consistent with the few previous airborne measurements. Dix et al. (2013) reported an IO VCD_{trop} of 2.49 and 2.91×10^{12} molec cm⁻² over the central Pacific and Volkamer et al. (2015) found 2.1 and 2.5×10^{12} molec cm⁻² over the eastern Pacific; both studies probed tropical air in the northern hemisphere winter. The average IO VCD_{trop} above SPL demonstrates that iodine is widespread in the free troposphere, including over continents.

The significant day-to-day temporal variability in IO VCD_{trop} over the central continental U.S. $(0.7 \pm 0.5 \text{ to } 3.6 \pm 0.5 \times 10^{12} \text{ molec cm}^{-2})$ has not been previously observed. Our measurements also characterize IO VCD_{trop} for the first time in the spring. Information about iodine spatiotemporal variability in the free troposphere is extremely scarce. Two sources affecting free tropospheric IO variability are marine convection (Dix et al., 2013) and dust (Koenig et al., 2021; Puentedura et al., 2012). Regional-scale IO variability over the Eastern Pacific Ocean was systematically probed by Wang et al. (2015), who reported IO VCD_{trop} of $2.6-3.5 \times 10^{12}$ molec cm⁻² and 5.1×10^{12} molec cm⁻² in the southern hemisphere tropical and subtropical Pacific, respectively, during Austral summer. Some of this variability could be attributed to dust sources of iodine from the Sechura and Atacama deserts (Koenig et al., 2021), with regional impacts on ozone in the marine boundary layer and free troposphere. Puentedura et al. (2012) reported variability in IO dSCDs related to Saharan dust impacts in the free troposphere over Tenerife Island in the Eastern Atlantic; they did not attempt to retrieve IO VCD_{trop}. Elevated IO VCD_{trop} over SPL is related to rapid transport from the Pacific Ocean, consistent with marine convection upwind, and unrelated to immediate dust impacts.

Schönhardt et al. (2008) reported global satellite measurements of IO SCDs. Their analysis used a reference spectrum over the tropical Pacific, where airborne measurements indicate that there is a significant IO VCD_{trop} (Dix et al., 2013; Volkamer et al., 2015). Therefore, the satellite IO SCDs are lower limits and not directly comparable to our measurements.

4.2. Ozone Relevance

Iodine is responsible for a \sim 9% reduction in the total tropospheric ozone burden, and model-measurement agreement for IO profiles over the eastern tropical Pacific indicates that marine sources for IO are reasonably well-constrained (Wang et al., 2021). The consistent low bias in modeled IO compared to our observations, combined with the observed fast transport from over the Pacific Ocean, suggests that sinks for IO along the transport path may be overestimated. Additionally, iodine's contribution to tropospheric ozone destruction may be higher than currently estimated over continents. GEOS-Chem iodine chemistry has not been significantly updated since version 11-02-rc, with the implementation of Wang et al. (2021) in version 12.9 leaving the mechanism of Sherwen, Evans, et al. (2016) largely unchanged.

4.3. Implications for Atmospheric Mercury Oxidation

Iodine oxidation of mercury is deemed unimportant, and is therefore missing in atmospheric models, in part due to the lower Hg-I bond strength (7.8–10.9 kcal $\mathrm{mol^{-1}}$; Salter et al., 1986; Shepler et al., 2005; Cremer et al., 2008) compared to Hg-Br (15.8 kcal $\mathrm{mol^{-1}}$; Tellinghuisen & Ashmore, 1983) and Hg-OH (11.0 kcal $\mathrm{mol^{-1}}$; Dibble et al., 2020). The Hg-OH bond strength was previously thought to be too weak to lead to $\mathrm{Hg^{II}}$ formation, but the discovery that the reaction of $\mathrm{Hg^{I}}$ species with ozone is kinetically barrierless (Saiz-Lopez et al., 2020) has resulted in a re-evaluation of the global relevance of OH radicals to $\mathrm{Hg^{0}}_{(g)}$ oxidation (Castro et al., 2022; Shah et al., 2021). There is evidence suggesting that the reaction of $\mathrm{Hg^{0}}_{(g)}$ with I atom proceeds faster than with Br atom (Goodsite et al., 2004, 2012). In light of the larger than predicted amounts of tropospheric iodine over continents, the Hg-I bond strength and $\mathrm{Hg^{I}(I)_{(g)}}$ dissociation rate warrant re-evaluation.

Our box model results (Figure 3) show that I atoms may oxidize Hg^0 at rates rivaling Br atoms and OH radicals at cold temperatures typical of the free troposphere. This finding depends on the assumed reaction kinetics and Hg-I bond strength, both of which are highly uncertain. Our most conservative estimate, which uses a rate constant half as fast as the k_{Hg+Br} measured by Donohoue et al. (2006) for k_{Hg+I} and assumes an Hg-I bond strength of 8.0 kcal mol^{-1} , places iodine atoms at a contribution of 0.3%-19.6% to $Hg^{II}_{(g)}$ formation below 12 km (Br: 17.5%-81.9%; OH: 10.9%-81.8%; CI: <0.7%). Our least conservative estimate, which uses a rate constant twice

LEE ET AL. 8 of 13

as fast as the k_{Hg+Br} measured by Donohoue et al. (2006) for k_{Hg+I} and assumes an Hg-I bond strength of 11.0 kcal mol⁻¹, places iodine atoms at a contribution of 34.6%–63.1% to $Hg^{II}_{(g)}$ formation below 12 km (Br: 11.5%–32.8%; OH: 4.4%–53.6%; CI: <0.4%). These results are consistent with the observed correlation between mercury and iodine in aerosols in the lower stratosphere (Murphy et al., 2006), and suggest these correlations might have a mechanistic causal relationship. The inclusion of iodine radical oxidation of $Hg^{0}_{(g)}$ to Hg^{II} in atmospheric models is desirable, as is better knowledge of the reaction kinetics and better constraints on the tropospheric iodine distribution.

Data Availability Statement

All CU MAX-DOAS and dual-channel mercury system measurement data at SPL during April 2022 (measured trace gas SCD; and measured and GEOS-Chem simulated trace gas VCD_{trop}, VMR_{instr}; measured and GEOS-Chem simulated Hg⁰ & Hg^{II}) as well as the gas-phase mercury chemical box model constraints & output described in this study are publicly available at zenodo with a Creative Commons Attribution 4.0 license (Lee, Elgiar, et al., 2024). The HYSPLIT-STILT back trajectory simulations at SPL during April 2022 described in this study are publicly available at zenodo with a Creative Commons Attribution 4.0 license (Lee, Wilmot, et al., 2024). The long-term measurements of Hg⁰, Hg^{II}, trace gases, and meteorology at SPL, a subset of which are used in this study, are publicly available at zenodo with a Creative Commons Attribution 4.0 license (Gratz et al., 2024). Version 13.2.1 of the GEOS-Chem model was used to simulate atmospheric oxidant fields and is available via an MIT license (The International GEOS-Chem User Community, 2021). Version 12.8.0 of the GEOS-Chem model was used to simulate atmospheric mercury chemistry is available via an MIT license (The International GEOS-Chem User Community, 2020). Version 3.4.5 of the QDOAS spectral analysis software developed by the DOAS UV-VIS team at the Royal Belgian Institute for Space Aeronomy (BIRA-IASB) was used for all DOAS spectral analysis and is available via a BSD 3-clause type license (https://uv-vis.aeronomie.be/ software/QDOAS/index.php). Version 8.0.4.2 of the IGOR Pro software developed by WaveMetrics, Inc. was used for data analysis and is available via a commercial license (https://www.wavemetrics.com/products/ igorpro).

Acknowledgments

Funding from the U.S. National Science Foundation (AGS-1951513, AGS-1951514, AGS-1951515, AGS-1951632) is gratefully acknowledged. The Steamboat Ski Resort, Maria Garcia, Dan Gilchrist, and SPL staff provided logistical support. Caroline Womack and Jessica Haskins assisted with F0AM. The Global Modeling and Assimilation Office at NASA Goddard Space Flight Center provided MERRA-2 meteorological data. Thank you to the reviewers for suggestions and feedback.

References

- Alicke, B., Hebestreit, K., Stutz, J., & Platt, U. (1999). Iodine oxide in the marine boundary layer. *Nature*, 397(6720), 572–573. https://doi.org/10.1038/17508
- Allan, B. J., McFiggans, G., Plane, J. M. C., & Coe, H. (2000). Observations of iodine monoxide in the remote marine boundary layer. *Journal of Geophysical Research*, 105(D11), 14363–14369. https://doi.org/10.1029/1999JD901188
- Baccarini, A., Karlsson, L., Dommen, J., Duplessis, P., Vüllers, J., Brooks, I. M., et al. (2020). Frequent new particle formation over the high Arctic pack ice by enhanced iodine emissions. *Nature Communications*, 11(1), 4924. https://doi.org/10.1038/s41467-020-18551-0
- Bell, N., Hsu, L., Jacob, D. J., Schultz, M. G., Blake, D. R., Butler, J. H., et al. (2002). Methyl iodide: Atmospheric budget and use as a tracer of
- marine convection in global models. *Journal of Geophysical Research*, 107(D17). https://doi.org/10.1029/2001JD001151
 Borys, R., & Wetzel, M. (1997). Storm Peak Laboratory: A research, teaching, and service facility for the atmospheric sciences. *Bulletin of the*
- American Meteorological Society, 78(10), 2115–2123. https://doi.org/10.1175/1520-0477(1997)078%3C2115:SPLART%3E2.0.CO;2
 Carpenter, L. J., MacDonald, S. M., Shaw, M. D., Kumar, R., Saunders, R. W., Parthipan, R., et al. (2013). Atmospheric iodine levels influenced by sea surface emissions of inorganic iodine. Nature Geoscience, 6(2), 108–111. https://doi.org/10.1038/ngeo1687
- Castro, P. J., Kellö, V., Cernušák, I., & Dibble, T. S. (2022). Together, not separately, OH and O₃ oxidize Hg^(II) in the atmosphere. *The Journal of Physical Chemistry A*, 126(44), 8266–8279. https://doi.org/10.1021/acs.jpca.2c04364
- Coburn, S., Dix, B., Edgerton, E., Holmes, C. D., Kinnison, D., Liang, Q., et al. (2016). Mercury oxidation from bromine chemistry in the free troposphere over the southeastern US. *Atmospheric Chemistry and Physics*, 16(6), 3743–3760. https://doi.org/10.5194/acp-16-3743-2016
- Coburn, S., Dix, B., Sinreich, R., & Volkamer, R. (2011). The CU ground MAX-DOAS instrument: Characterization of RMS noise limitations and first measurements near Pensacola, FL of BrO, IO, and CHOCHO. Atmospheric Measurement Techniques, 4(11), 2421–2439. https://doi. org/10.5194/amt-4-2421-2011
- Cremer, D., Kraka, E., & Filatov, M. (2008). Bonding in mercury molecules described by the normalized elimination of the small component and coupled cluster theory. *ChemPhysChem*, 9(17), 2510–2521. https://doi.org/10.1002/cphc.200800510
- Cuevas, C. A., Maffezzoli, N., Corella, J. P., Spolaor, A., Vallelonga, P., Kjær, H. A., et al. (2018). Rapid increase in atmospheric iodine levels in the North Atlantic since the mid-20th century. *Nature Communications*, 9(1), 1452. https://doi.org/10.1038/s41467-018-03756-1
- Derry, E. J., Elgiar, T. R., Wilmot, T. Y., Hoch, N. W., Hirshorn, N. S., Weiss-Penzias, P., et al. (2024). Elevated oxidized mercury in the free troposphere: Analytical advances and application at a remote continental mountaintop site. Atmospheric Chemistry and Physics, 24(16), 9615–9643. https://doi.org/10.5194/acp-24-9615-2024
- Deutschmann, T., Beirle, S., Frieß, U., Grzegorski, M., Kern, C., Kritten, L., et al. (2011). The Monte Carlo atmospheric radiative transfer model McArtim: Introduction and validation of Jacobians and 3D features. *Journal of Quantitative Spectroscopy and Radiative Transfer*, 112(6), 1119–1137. https://doi.org/10.1016/j.jqsrt.2010.12.009
- Dibble, T. S., Tetu, H. L., Jiao, Y., Thackray, C. P., & Jacob, D. J. (2020). Modeling the OH-initiated oxidation of mercury in the global atmosphere without violating physical laws. *The Journal of Physical Chemistry A, 124*(2), 444–453. https://doi.org/10.1021/acs.jpca.9b10121

LEE ET AL. 9 of 13

- Dix, B., Baidar, S., Bresch, J. F., Hall, S. R., Schmidt, K. S., Wang, S., & Volkamer, R. (2013). Detection of iodine monoxide in the tropical free troposphere. *Proceedings of the National Academy of Sciences of the United States of America*, 110(6), 2035–2040. https://doi.org/10.1073/pnas.1212386110
- Donohoue, D. L., Bauer, D., Cossairt, B., & Hynes, A. J. (2006). Temperature and pressure dependent rate coefficients for the reaction of Hg with Br and the reaction of Br with Br: A pulsed laser photolysis-pulsed laser induced fluorescence study. *The Journal of Physical Chemistry A*, 110(21), 6623–6632. https://doi.org/10.1021/jp054688j
- Elgiar, T. R., Lyman, S. N., Andron, T. D., Gratz, L., Hallar, A. G., Horvat, M., et al. (2024). Traceable calibration of atmospheric oxidized mercury measurements. *Environmental Science & Technology*, 58(24), 10706–10716. acs.est.4c02209. https://doi.org/10.1021/acs.est.4c02209
- Fain, X., Obrist, D., Hallar, A. G., McCubbin, I., & Rahn, T. (2009). High levels of reactive gaseous mercury observed at a high elevation research laboratory in the Rocky Mountains. Atmospheric Chemistry and Physics, 9(20), 8049–8060. https://doi.org/10.5194/acp-9-8049-2009
- Finkenzeller, H., Iyer, S., He, X.-C., Simon, M., Koenig, T. K., Lee, C. F., et al. (2023). The gas-phase formation mechanism of iodic acid as an atmospheric aerosol source. *Nature Chemistry*, 15(1), 129–135. https://doi.org/10.1038/s41557-022-01067-z
- Frieß, U., Deutschmann, T., Gilfedder, B. S., Weller, R., & Platt, U. (2010). Iodine monoxide in the Antarctic snowpack. Atmospheric Chemistry and Physics, 10(5), 2439–2456. https://doi.org/10.5194/acp-10-2439-2010
- Furneaux, K. L., Whalley, L. K., Heard, D. E., Atkinson, H. M., Bloss, W. J., Flynn, M. J., et al. (2010). Measurements of iodine monoxide at a
- semi polluted coastal location. Atmospheric Chemistry and Physics, 10(8), 3645–3663. https://doi.org/10.5194/acp-10-3645-2010
 Gielen, C., Van Roozendael, M., Hendrick, F., Pinardi, G., Vlemmix, T., De Bock, V., et al. (2014). A simple and versatile cloud-screening
- method for MAX-DOAS retrievals. Atmospheric Measurement Techniques, 7(10), 3509–3527. https://doi.org/10.5194/amt-7-3509-2014
 Gómez Martín, J. C., Lewis, T. R., James, A. D., Saiz-Lopez, A., & Plane, J. M. C. (2022). Insights into the chemistry of iodine new particle formation: The role of iodine oxides and the source of iodic acid. Journal of the American Chemical Society, 144(21), 9240–9253. https://doi.
- org/10.1021/jacs.1c12957

 Gómez Martín, J. C., Mahajan, A. S., Hay, T. D., Prados-Román, C., Ordóñez, C., MacDonald, S. M., et al. (2013). Iodine chemistry in the eastern Pacific marine boundary layer. *Journal of Geophysical Research: Atmospheres*, 118(2), 887–904. https://doi.org/10.1002/jgrd.50132
- Goodsite, M. E., Plane, J. M. C., & Skov, H. (2004). A theoretical study of the oxidation of Hg⁰ to HgBr₂ in the troposphere. *Environmental Science & Technology*, 38(6), 1772–1776. https://doi.org/10.1021/es034680s
- Goodsite, M. E., Plane, J. M. C., & Skov, H. (2012). Correction to a theoretical study of the oxidation of Hg⁰ to HgBr₂ in the troposphere. *Environmental Science & Technology*, 46(9), 5262. https://doi.org/10.1021/es301201c
- Environmental Science & Technology, 46(9), 5262. https://doi.org/10.1021/es301201c
 Gratz, L., Lyman, S., Elgiar, T., Hallar, A. G., & Volkamer, R. (2024). Measurements of atmospheric mercury, trace gases, aerosols, and
- meteorology at Storm Peak Laboratory, Colorado, in 2021 and 2022 (version 1) [dataset]. Zenodo. https://doi.org/10.5281/ZENODO.10699270 Großmann, K., Frieß, U., Peters, E., Wittrock, F., Lampel, J., Yilmaz, S., et al. (2013). Iodine monoxide in the Western Pacific marine boundary layer. Atmospheric Chemistry and Physics, 13(6), 3363–3378. https://doi.org/10.5194/acp-13-3363-2013
- Hallar, A. G., Petersen, R., McCubbin, I. B., Lowenthal, D., Lee, S., Andrews, E., & Yu, F. (2016). Climatology of new particle formation and corresponding precursors at Storm Peak Laboratory. *Aerosol and Air Quality Research*, 16(3), 816–826. https://doi.org/10.4209/aaqr.2015.05.
- He, X.-C., Tham, Y. J., Dada, L., Wang, M., Finkenzeller, H., Stolzenburg, D., et al. (2021). Role of iodine oxoacids in atmospheric aerosol nucleation. *Science*, 371(6529), 589–595. https://doi.org/10.1126/science.abe0298
- Hendrick, F., Van Roozendael, M., Chipperfield, M. P., Dorf, M., Goutail, F., Yang, X., et al. (2007). Retrieval of stratospheric and tropospheric BrO profiles and columns using ground-based zenith-sky DOAS observations at Harestua, 60° N. *Atmospheric Chemistry and Physics*, 7(18), 4869–4885. https://doi.org/10.5194/acp-7-4869-2007
- Inamdar, S., Tinel, L., Chance, R., Carpenter, L. J., Sabu, P., Chacko, R., et al. (2020). Estimation of reactive inorganic iodine fluxes in the Indian and Southern Ocean marine boundary layer. Atmospheric Chemistry and Physics, 20(20), 12093–12114. https://doi.org/10.5194/acp-20-12093-2020
- Inness, A., Ades, M., Agustí-Panareda, A., Barré, J., Benedictow, A., Blechschmidt, A.-M., et al. (2019). The CAMS reanalysis of atmospheric composition. Atmospheric Chemistry and Physics, 19(6), 3515–3556. https://doi.org/10.5194/acp-19-3515-2019
- Jones, C. E., Hornsby, K. E., Sommariva, R., Dunk, R. M., Von Glasow, R., McFiggans, G., & Carpenter, L. J. (2010). Quantifying the contribution of marine organic gases to atmospheric iodine. *Geophysical Research Letters*, 37(18), 2010GL043990. https://doi.org/10.1029/ 2010GL043990
- Koenig, T. K., Baidar, S., Campuzano-Jost, P., Cuevas, C. A., Dix, B., Fernandez, R. P., et al. (2020). Quantitative detection of iodine in the stratosphere. Proceedings of the National Academy of Sciences of the United Staets of America, 117(4), 1860–1866. https://doi.org/10.1073/pnas.1916828117
- Koenig, T. K., Volkamer, R., Apel, E. C., Bresch, J. F., Cuevas, C. A., Dix, B., et al. (2021). Ozone depletion due to dust release of iodine in the free troposphere. *Science Advances*, 7(52), eabi6544. https://doi.org/10.1126/sciadv.abi6544
- Lee, C. F., Elgiar, T., David, L. M., Wilmot, K., Reza, M., Hirshorn, N., et al. (2024). Measurements and model simulations of iodine monoxide (IO) radical, water vapor (H₂O), nitrogen dioxide (NO₂) radical, formaldehyde (HCHO), gaseous elemental mercury (Hg⁰), and oxidized mercury (Hg^{II}) at Storm Peak Laboratory, Colorado, during April 2022 [Dataset]. Zenodo. https://doi.org/10.5281/ZENODO.10805549
- Lee, C. F., Wilmot, K., Lin, J. C., Lyman, S. N., Hallar, A. G., Gratz, L. E., & Volkamer, R. (2024). 24-hour HYSPLIT-STILT back-trajectories initialized at Storm Peak Laboratory, Colorado from April 1, 2022 to May 1, 2022 [Dataset]. Zenodo. https://doi.org/10.5281/ZENODO. 10806478
- Legrand, M., McConnell, J. R., Preunkert, S., Arienzo, M., Chellman, N., Gleason, K., et al. (2018). Alpine ice evidence of a three-fold increase in atmospheric iodine deposition since 1950 in Europe due to increasing oceanic emissions. *Proceedings of the National Academy of Sciences of the United States of America*, 115(48), 12136–12141. https://doi.org/10.1073/pnas.1809867115
- Lin, J. C., Gerbig, C., Wofsy, S. C., Andrews, A. E., Daube, B. C., Davis, K. J., & Grainger, C. A. (2003). A near-field tool for simulating the upstream influence of atmospheric observations: The Stochastic Time-Inverted Lagrangian Transport (STILT) model. *Journal of Geophysical Research*, 108(D16), 2002JD003161. https://doi.org/10.1029/2002JD003161
- Loughner, C. P., Fasoli, B., Stein, A. F., & Lin, J. C. (2021). Incorporating features from the Stochastic Time-Inverted Lagrangian Transport (STILT) model into the Hybrid Single-Particle Lagrangian Integrated Trajectory (HYSPLIT) model: A unified dispersion model for time-forward and time-reversed applications. *Journal of Applied Meteorology and Climatology*. https://doi.org/10.1175/JAMC-D-20-0158.1
- Lyman, S. N., Gratz, L. E., Dunham-Cheatham, S. M., Gustin, M. S., & Luippold, A. (2020). Improvements to the accuracy of atmospheric oxidized mercury measurements. *Environmental Science & Technology*, 54(21), 13379–13388. https://doi.org/10.1021/acs.est.0c02747

LEE ET AL. 10 of 13

- MacDonald, S. M., Gómez Martín, J. C., Chance, R., Warriner, S., Saiz-Lopez, A., Carpenter, L. J., & Plane, J. M. C. (2014). A laboratory characterisation of inorganic iodine emissions from the sea surface: Dependence on oceanic variables and parameterisation for global modelling. Atmospheric Chemistry and Physics, 14(11), 5841–5852. https://doi.org/10.5194/acp-14-5841-2014
- Mahajan, A. S., Gómez Martín, J. C., Hay, T. D., Royer, S.-J., Yvon-Lewis, S., Liu, Y., et al. (2012). Latitudinal distribution of reactive iodine in the Eastern Pacific and its link to open ocean sources. *Atmospheric Chemistry and Physics*, 12(23), 11609–11617. https://doi.org/10.5194/acp-12-11609-2012.
- Mahajan, A. S., Shaw, M., Oetjen, H., Hornsby, K. E., Carpenter, L. J., Kaleschke, L., et al. (2010). Evidence of reactive iodine chemistry in the Arctic boundary layer. *Journal of Geophysical Research*, 115(D20), 2009JD013665. https://doi.org/10.1029/2009JD013665
- Miller, M. B., Dunham-Cheatham, S. M., Gustin, M. S., & Edwards, G. C. (2019). Evaluation of cation exchange membrane performance under exposure to high Hg0 and HgBr2 concentrations. Atmospheric Measurement Techniques, 12(2), 1207–1217. https://doi.org/10.5194/amt-12-1207-2019
- Murphy, D. M., Hudson, P. K., Thomson, D. S., Sheridan, P. J., & Wilson, J. C. (2006). Observations of mercury-containing aerosols. *Environmental Science & Technology*, 40(10), 3163–3167. https://doi.org/10.1021/es052385x
- Obrist, D., Hallar, A. G., McCubbin, I., Stephens, B. B., & Rahn, T. (2008). Atmospheric mercury concentrations at Storm Peak Laboratory in the Rocky Mountains: Evidence for long-range transport from Asia, boundary layer contributions, and plant mercury uptake. *Atmospheric Environment*, 42(33), 7579–7589. https://doi.org/10.1016/j.atmosenv.2008.06.051
- O'Dowd, C. D., Jimenez, J. L., Bahreini, R., Flagan, R. C., Seinfeld, J. H., Hämeri, K., et al. (2002). Marine aerosol formation from biogenic iodine emissions. *Nature*, 417(6889), 632–636. https://doi.org/10.1038/nature00775
- Ordóñez, C., Lamarque, J.-F., Tilmes, S., Kinnison, D. E., Atlas, E. L., Blake, D. R., et al. (2012). Bromine and iodine chemistry in a global chemistry-climate model: Description and evaluation of very short-lived oceanic sources. Atmospheric Chemistry and Physics, 12(3), 1423–1447. https://doi.org/10.5194/acp-12-1423-2012
- Ortega, I., Berg, L. K., Ferrare, R. A., Hair, J. W., Hostetler, C. A., & Volkamer, R. (2016). Elevated aerosol layers modify the O2–O2 absorption measured by ground-based MAX-DOAS. *Journal of Quantitative Spectroscopy and Radiative Transfer*, 176, 34–49. https://doi.org/10.1016/j. iosrt.2016.02.021
- Platt, U., & Stutz, J. (2008). Differential optical absorption spectroscopy: Principles and applications. Springer.
- Prados-Roman, C., Cuevas, C. A., Hay, T., Fernandez, R. P., Mahajan, A. S., Royer, S.-J., et al. (2015). Iodine oxide in the global marine boundary layer. Atmospheric Chemistry and Physics, 15(2), 583–593. https://doi.org/10.5194/acp-15-583-2015
- Puentedura, O., Gil, M., Saiz-Lopez, A., Hay, T., Navarro-Comas, M., Gómez-Pelaez, A., et al. (2012). Iodine monoxide in the north subtropical free troposphere. Atmospheric Chemistry and Physics, 12(11), 4909–4921. https://doi.org/10.5194/acp-12-4909-2012
- Read, K. A., Mahajan, A. S., Carpenter, L. J., Evans, M. J., Faria, B. V. E., Heard, D. E., et al. (2008). Extensive halogen-mediated ozone destruction over the tropical Atlantic Ocean. *Nature*, 453(7199), 1232–1235. https://doi.org/10.1038/nature07035
- Rodgers, C. D. (2000). Inverse methods for atmospheric sounding: Theory and practice (Vol. 2). WORLD SCIENTIFIC. https://doi.org/10.1142/
- Saiz-Lopez, A., Fernandez, R. P., Ordóñez, C., Kinnison, D. E., Gómez Martín, J. C., Lamarque, J.-F., & Tilmes, S. (2014). Iodine chemistry in the troposphere and its effect on ozone. Atmospheric Chemistry and Physics, 14(23), 13119–13143. https://doi.org/10.5194/acp-14-13119-2014
- Saiz-Lopez, A., Lamarque, J.-F., Kinnison, D. E., Tilmes, S., Ordóñez, C., Orlando, J. J., et al. (2012). Estimating the climate significance of halogen-driven ozone loss in the tropical marine troposphere. Atmospheric Chemistry and Physics, 12(9), 3939–3949. https://doi.org/10.5194/ acp-12-3939-2012
- Saiz-Lopez, A., Sitkiewicz, S. P., Roca-Sanjuán, D., Oliva-Enrich, J. M., Dávalos, J. Z., Notario, R., et al. (2018). Photoreduction of gaseous oxidized mercury changes global atmospheric mercury speciation, transport and deposition. *Nature Communications*, 9(1), 4796. https://doi.org/10.1038/s41467-018-07075-3
- Saiz-Lopez, A., Travnikov, O., Sonke, J. E., Thackray, C. P., Jacob, D. J., Carmona-García, J., et al. (2020). Photochemistry of oxidized Hg^(I) and Hg^(II) species suggests missing mercury oxidation in the troposphere. Proceedings of the National Academy of Sciences of the United States of America, 117(49), 30949–30956. https://doi.org/10.1073/pnas.1922486117
- Salter, C., Tellinghuisen, P. C., Ashmore, J. G., & Tellinghuisen, J. (1986). The emission spectrum of 200Hg127I. Journal of Molecular Spectroscopy, 120(2), 334–358. https://doi.org/10.1016/0022-2852(86)90009-3
- Schönhardt, A., Begoin, M., Richter, A., Wittrock, F., Kaleschke, L., Gómez Martín, J. C., & Burrows, J. P. (2012). Simultaneous satellite observations of IO and BrO over Antarctica. *Atmospheric Chemistry and Physics*, 12(14), 6565–6580. https://doi.org/10.5194/acp-12-6565-2012
- Schönhardt, A., Richter, A., Theys, N., & Burrows, J. P. (2017). Space-based observation of volcanic iodine monoxide. Atmospheric Chemistry and Physics, 17(7), 4857–4870. https://doi.org/10.5194/acp-17-4857-2017
- Schönhardt, A., Richter, A., Wittrock, F., Kirk, H., Oetjen, H., Roscoe, H. K., & Burrows, J. P. (2008). Observations of iodine monoxide columns from satellite. *Atmospheric Chemistry and Physics*, 8(3), 637–653. https://doi.org/10.5194/acp-8-637-2008
- Shah, V., Jacob, D. J., Thackray, C. P., Wang, X., Sunderland, E. M., Dibble, T. S., et al. (2021). Improved mechanistic model of the atmospheric redox chemistry of mercury. *Environmental Science & Technology*, 55(21), 14445–14456. https://doi.org/10.1021/acs.est.1c03160
- Shepler, B. C., Balabanov, N. B., & Peterson, K. A. (2005). Ab initio thermochemistry involving heavy atoms: An investigation of the reactions Hg + IX (X = I, Br, Cl, O). The Journal of Physical Chemistry A, 109(45), 10363–10372. https://doi.org/10.1021/jp0541617
- Sherwen, T., Evans, M. J., Carpenter, L. J., Andrews, S. J., Lidster, R. T., Dix, B., et al. (2016). Iodine's impact on tropospheric oxidants: A global model study in GEOS-chem. Atmospheric Chemistry and Physics, 16(2), 1161–1186. https://doi.org/10.5194/acp-16-1161-2016
- Sherwen, T., Evans, M. J., Carpenter, L. J., Schmidt, J. A., & Mickley, L. J. (2017). Halogen chemistry reduces tropospheric O₃ radiative forcing. Atmospheric Chemistry and Physics, 17(2), 1557–1569. https://doi.org/10.5194/acp-17-1557-2017
- Sherwen, T., Schmidt, J. A., Evans, M. J., Carpenter, L. J., Großmann, K., Eastham, S. D., et al. (2016). Global impacts of tropospheric halogens (Cl, Br, I) on oxidants and composition in GEOS-Chem. *Atmospheric Chemistry and Physics*, 16(18), 12239–12271. https://doi.org/10.5194/acp-16-12239-2016
- Sipilä, M., Sarnela, N., Jokinen, T., Henschel, H., Junninen, H., Kontkanen, J., et al. (2016). Molecular-scale evidence of aerosol particle formation via sequential addition of HIO3. *Nature*, 537(7621), 532–534. https://doi.org/10.1038/nature19314
- Sive, B. C., Varner, R. K., Mao, H., Blake, D. R., Wingenter, O. W., & Talbot, R. (2007). A large terrestrial source of methyl iodide. *Geophysical Research Letters*, 34(17), 2007GL030528. https://doi.org/10.1029/2007GL030528
- Spietz, P., Gómez Martín, J. C., & Burrows, J. P. (2005). Spectroscopic studies of the 12/O3 photochemistry. *Journal of Photochemistry and Photobiology A: Chemistry*, 176(1–3), 50–67. https://doi.org/10.1016/j.jphotochem.2005.08.023

LEE ET AL. 11 of 13

- Spinei, E., Cede, A., Herman, J., Mount, G. H., Eloranta, E., Morley, B., et al. (2015). Ground-based direct-sun DOAS and airborne MAX-DOAS measurements of the collision-induced oxygen complex, O2O2, absorption with significant pressure and temperature differences. *Atmospheric Measurement Techniques*, 8(2), 793–809. https://doi.org/10.5194/amt-8-793-2015
- Takashima, H., Kanaya, Y., Kato, S., Friedrich, M. M., Van Roozendael, M., Taketani, F., et al. (2022). Full latitudinal marine atmospheric measurements of iodine monoxide. Atmospheric Chemistry and Physics, 22(6), 4005–4018. https://doi.org/10.5194/acp-22-4005-2022
- Tellinghuisen, J., & Ashmore, J. G. (1983). Mixed representations for diatomic spectroscopic data: Application to HgBr. Chemical Physics Letters, 102(1), 10–16. https://doi.org/10.1016/0009-2614(83)80647-2
- The International GEOS-Chem User Community. (2020). geoschem/geos-chem: GEOS-Chem 12.8.0 (Version 12.8.0) [Software]. Zenodo. https://doi.org/10.5281/ZENODO.3784796
- The International GEOS-Chem User Community. (2021). geoschem/GCClassic: GEOS-Chem 13.2.1 (Version 13.2.1) [Software]. Zenodo. https://doi.org/10.5281/ZENODO.5500717
- Tirpitz, J.-L., Frieß, U., Hendrick, F., Alberti, C., Allaart, M., Apituley, A., et al. (2021). Intercomparison of MAX-DOAS vertical profile retrieval algorithms: Studies on field data from the CINDI-2 campaign. *Atmospheric Measurement Techniques*, 14(1), 1–35. https://doi.org/10.5194/amt-14-1-2021
- Volkamer, R., Baidar, S., Campos, T. L., Coburn, S., DiGangi, J. P., Dix, B., et al. (2015). Aircraft measurements of BrO, IO, glyoxal, NO₂, H₂O, O₂–O₂ and aerosol extinction profiles in the tropics: Comparison with aircraft-/ship-based in situ and lidar measurements. *Atmospheric Measurement Techniques*, 8(5), 2121–2148. https://doi.org/10.5194/amt-8-2121-2015
- Wagner, T., Apituley, A., Beirle, S., Dörner, S., Friess, U., Remmers, J., & Shaiganfar, R. (2014). Cloud detection and classification based on MAX-DOAS observations. Atmospheric Measurement Techniques, 7(5), 1289–1320. https://doi.org/10.5194/amt-7-1289-2014
- Wagner, T., Beirle, S., Benavent, N., Bösch, T., Chan, K. L., Donner, S., et al. (2019). Is a scaling factor required to obtain closure between measured and modelled atmospheric O4 absorptions? An assessment of uncertainties of measurements and radiative transfer simulations for 2 selected days during the MAD-CAT campaign. Atmospheric Measurement Techniques, 12(5), 2745–2817. https://doi.org/10.5194/amt-12-2745-2019
- Wang, F., Saiz-Lopez, A., Mahajan, A. S., Gómez Martín, J. C., Armstrong, D., Lemes, M., et al. (2014). Enhanced production of oxidised mercury over the tropical Pacific Ocean: A key missing oxidation pathway. Atmospheric Chemistry and Physics, 14(3), 1323–1335. https://doi. org/10.5194/acp-14-1323-2014
- Wang, S., Schmidt, J. A., Baidar, S., Coburn, S., Dix, B., Koenig, T. K., et al. (2015). Active and widespread halogen chemistry in the tropical and subtropical free troposphere. Proceedings of the National Academy of Sciences of the United States of America, 112(30), 9281–9286. https://doi.org/10.1073/pnas.1505142112
- Wang, X., Jacob, D. J., Downs, W., Zhai, S., Zhu, L., Shah, V., et al. (2021). Global tropospheric halogen (Cl, Br, I) chemistry and its impact on oxidants. *Atmospheric Chemistry and Physics*, 21(18), 13973–13996. https://doi.org/10.5194/acp-21-13973-2021
- Wennberg, P. O., Brault, J. W., Hanisco, T. F., Salawitch, R. J., & Mount, G. H. (1997). The atmospheric column abundance of IO: Implications for stratospheric ozone. *Journal of Geophysical Research*, 102(D7), 8887–8898. https://doi.org/10.1029/96JD03712
- Whalley, L. K., Furneaux, K. L., Gravestock, T., Atkinson, H. M., Bale, C. S. E., Ingham, T., et al. (2007). Detection of iodine monoxide radicals in the marine boundary layer using laser induced fluorescence spectroscopy. *Journal of Atmospheric Chemistry*, 58(1), 19–39. https://doi.org/10.1007/s10874-007-9075-9
- Williams, J., Gros, V., Atlas, E., Maciejczyk, K., Batsaikhan, A., Schöler, H. F., et al. (2007). Possible evidence for a connection between methyl iodide emissions and Saharan dust. *Journal of Geophysical Research*, 112(D7), 2005JD006702. https://doi.org/10.1029/2005JD006702
- Wittrock, F., Müller, R., Richter, A., Bovensmann, H., & Burrows, J. P. (2000). Measurements of iodine monoxide (IO) above Spitsbergen. Geophysical Research Letters, 27(10), 1471–1474. https://doi.org/10.1029/1999GL011146
- Wolfe, G. M., Marvin, M. R., Roberts, S. J., Travis, K. R., & Liao, J. (2016). The framework for 0-D atmospheric modeling (F0AM) v3.1. Geoscientific Model Development, 9(9), 3309–3319. https://doi.org/10.5194/gmd-9-3309-2016
- Zhao, X., Hou, X., & Zhou, W. (2019). Atmospheric iodine (127I and 129I) record in spruce tree rings in the Northeast Qinghai-Tibet Plateau. Environmental Science & Technology, 53(15), 8706–8714. https://doi.org/10.1021/acs.est.9b01160

References From the Supporting Information

- Bosilovich, M. G., Robertson, F. R., Takacs, L., Molod, A., & Mocko, D. (2017). Atmospheric water balance and variability in the MERRA-2 reanalysis. *Journal of Climate*, 30(4), 1177–1196. https://doi.org/10.1175/JCLI-D-16-0338.1
- Chance, K., & Kurucz, R. L. (2010). An improved high-resolution solar reference spectrum for earth's atmosphere measurements in the ultraviolet, visible, and near infrared. *Journal of Quantitative Spectroscopy and Radiative Transfer*, 111(9), 1289–1295. https://doi.org/10.1016/j.jqsrt.2010.01.036
- Cheung, N.-H., & Cool, T. A. (1979). Franck-Condon factors and r-centroids for the B2Σ-X2Σ systems of HgCl, HgBr, and HgI. Journal of Ouantitative Spectroscopy and Radiative Transfer, 21(5), 397–432. https://doi.org/10.1016/0022-4073(79)90002-5
- Dowell, D. C., Alexander, C. R., James, E. P., Weygandt, S. S., Benjamin, S. G., Manikin, G. S., et al. (2022). The high-resolution rapid refresh (HRRR): An hourly updating convection-allowing forecast model. Part I: Motivation and system description. *Weather and Forecasting*, 37(8), 1371–1395. https://doi.org/10.1175/WAF-D-21-0151.1
- Finkenzeller, H., & Volkamer, R. (2022). O₂–O₂ CIA in the gas phase: Cross-section of weak bands, and continuum absorption between 297–500 nm. *Journal of Quantitative Spectroscopy and Radiative Transfer*, 279, 108063. https://doi.org/10.1016/j.jqsrt.2021.108063
- Fleischmann, O. C., Hartmann, M., Burrows, J. P., & Orphal, J. (2004). New ultraviolet absorption cross-sections of BrO at atmospheric temperatures measured by time-windowing Fourier transform spectroscopy. *Journal of Photochemistry and Photobiology A: Chemistry*, 168(1–2), 117–132. https://doi.org/10.1016/j.jphotochem.2004.03.026
- Giglio, L., Randerson, J. T., & Van Der Werf, G. R. (2013). Analysis of daily, monthly, and annual burned area using the fourth-generation global fire emissions database (GFED4). *Journal of Geophysical Research: Biogeosciences*, 118(1), 317–328. https://doi.org/10.1002/jgrg.20042
- Guenther, A. B., Jiang, X., Heald, C. L., Sakulyanontvittaya, T., Duhl, T., Emmons, L. K., & Wang, X. (2012). The Model of Emissions of Gases and Aerosols from Nature version 2.1 (MEGAN2.1): An extended and updated framework for modeling biogenic emissions. Geoscientific Model Development, 5(6), 1471–1492. https://doi.org/10.5194/gmd-5-1471-2012
- Hoesly, R. M., Smith, S. J., Feng, L., Klimont, Z., Janssens-Maenhout, G., Pitkanen, T., et al. (2018). Historical (1750–2014) anthropogenic emissions of reactive gases and aerosols from the Community Emissions Data System (CEDS). Geoscientific Model Development, 11(1), 369–408. https://doi.org/10.5194/gmd-11-369-2018

LEE ET AL. 12 of 13

- Lampel, J., Frieß, U., & Platt, U. (2015). The impact of vibrational Raman scattering of air on DOAS measurements of atmospheric trace gases. Atmospheric Measurement Techniques, 8(9), 3767–3787. https://doi.org/10.5194/amt-8-3767-2015
- Meller, R., & Moortgat, G. K. (2000). Temperature dependence of the absorption cross sections of formaldehyde between 223 and 323 K in the wavelength range 225–375 nm. *Journal of Geophysical Research*, 105(D6), 7089–7101. https://doi.org/10.1029/1999JD901074
- Pukīte, J., & Wagner, T. (2016). Quantification and parametrization of non-linearity effects by higher-order sensitivity terms in scattered light differential optical absorption spectroscopy. Atmospheric Measurement Techniques, 9(5), 2147–2177. https://doi.org/10.5194/amt-9-2147-2016
- Rothman, L. S., Gordon, I. E., Babikov, Y., Barbe, A., Chris Benner, D., Bernath, P. F., et al. (2013). The HITRAN2012 molecular spectroscopic database. *Journal of Quantitative Spectroscopy and Radiative Transfer*, 130, 4–50. https://doi.org/10.1016/j.jqsrt.2013.07.002
- Rothman, L. S., Gordon, I. E., Barber, R. J., Dothe, H., Gamache, R. R., Goldman, A., et al. (2010). HITEMP, the high-temperature molecular spectroscopic database. *Journal of Quantitative Spectroscopy and Radiative Transfer*, 111(15), 2139–2150. https://doi.org/10.1016/j.jqsrt. 2010.05.001
- Serdyuchenko, A., Gorshelev, V., Weber, M., Chehade, W., & Burrows, J. P. (2014). High spectral resolution ozone absorption cross-sections Part 2: Temperature dependence. *Atmospheric Measurement Techniques*, 7(2), 625–636. https://doi.org/10.5194/amt-7-625-2014
- Shah, V., Jacob, D. J., Dang, R., Lamsal, L. N., Strode, S. A., Steenrod, S. D., et al. (2023). Nitrogen oxides in the free troposphere: Implications for tropospheric oxidants and the interpretation of satellite NO₂ measurements. *Atmospheric Chemistry and Physics*, 23(2), 1227–1257. https://doi.org/10.5194/acp-23-1227-2023
- Thalman, R., & Volkamer, R. (2013). Temperature dependent absorption cross-sections of O₂–O₂ collision pairs between 340 and 630 nm and at atmospherically relevant pressure. *Physical Chemistry Chemical Physics*, 15(37), 15371. https://doi.org/10.1039/c3cp50968k
- Vandaele, A. C., Hermans, C., Simon, P. C., Carleer, M., Colin, R., Fally, S., et al. (1998). Measurements of the NO₂ absorption cross-section from 42 000 cm⁻¹ to 10 000 cm⁻¹ (238–1000 nm) at 220 K and 294 K. *Journal of Quantitative Spectroscopy and Radiative Transfer*, 59(3–5), 171–184. https://doi.org/10.1016/S0022-4073(97)00168-4
- Wieland, K. (1960). Bandensysteme B (2Σ+) \rightarrow X (2Σ+) und Dissoziationswerte der Radikale HgJ und HgBr. Zeitschrift Für Elektrochemie, Berichte Der Bunsengesellschaft Für Physikalische Chemie, 64(5), 761–769. https://doi.org/10.1002/bbpc.196000043

LEE ET AL. 13 of 13